Water oxidation kinetics of nanoporous $BiVO_4$ photoanodes functionalised with nickel/iron oxyhydroxide electrocatalysts

Laia Francàs,[1†] Shababa Selim,[1†] Sacha Corby,[1] Dongho Lee,[2] Camilo A. Mesa,[1] Ernest Pastor,[1] Kyoung-Shin Choi,[2] James R. Durrant[1]*

1. Department of Chemistry, Imperial College London, White City Campus, London W12 0BZ, United Kingdom
2. Department of Chemistry, University of Wisconsin-Madison, Madison, Wisconsin 53706, United States

[†]Authors contributed equally.

*corresponding author: j.durrant@imperial.ac.uk

Abstract

In this work, spectroelectrochemical techniques are employed to analyse the catalytic water oxidation performance of a series of three nickel/iron oxyhydroxide electrocatalysts deposited on FTO and $BiVO_4$, at neutral pH. Similar electrochemical water oxidation performance is observed for each of the FeOOH, Ni(Fe)OOH and FeOOHNiOOH electrocatalysts studied, which is found to result from a balance between degree of charge accumulation and rate of water oxidation. Once added onto $BiVO_4$ photoanodes, a large enhancement in the water oxidation photoelectrochemical performance is observed in comparison to the un-modified $BiVO_4$. To understand the origin of this enhancement, the films were evaluated through time-resolved optical spectroscopic techniques, allowing comparisons between electrochemical and photoelectrochemical water oxidation. For all three catalysts, fast hole transfer from $BiVO_4$ to the catalyst is observed in the transient absorption data. Using operando photoinduced absorption measurements, we find that water oxidation is driven by oxidised states within the catalyst layer, following hole transfer from $BiVO_4$. This charge transfer is correlated with a suppression of recombination losses which result in remarkably enhanced water oxidation performance relative to un-modified $BiVO_4$. Moreover, despite similar electrocatalytic performance of all three electrocatalysts, we show that variations in water oxidation performance observed among the $BiVO_4$/MOOH photoanodes stem from differences in photoelectrochemical and electrochemical charge accumulation in the catalyst layers. Under illumination, the amount of accumulated charge in the catalyst is driven by the injection of photogenerated holes from $BiVO_4$, which is further affected by the recombination loss at the $BiVO_4$/MOOH interface, and thus leads to deviations from their behaviour as standalone electrocatalysts.

Introduction

Artificial photosynthesis employing photoelectrochemical or photocatalytic systems is attracting increasing interest for the sustainable synthesis of molecular fuels and chemicals.[1–4] Metal oxides are widely studied as light absorbing materials for such solar-to-fuel systems, particularly for the challenging water oxidation reaction.[5,6] This interest is derived particularly from their stability under the highly oxidising conditions required to drive this reaction. However, the performance of such metal oxide-based photoelectrodes is generally limited by recombination losses; in particular, competing surface recombination losses (also known as back electron/hole recombination) due to the slow rate of water oxidation, can be very significant.[7–12] One widely used approach to reduce such losses is the addition of water oxidation catalyst layers on the photoanode surface, which can lead to an enhancement in performance.[12–16] However, the selection of suitable catalysts is challenging as the requirements for efficient photoanode performance is likely to be different from the requirements for efficient, dark electrocatalysis. This is because, unlike electrocatalytic systems, driven by a voltage source, photoanodes utilise photogenerated holes, which are subject to electron-hole recombination losses at the photoanode/electrocatalyst/electrolyte interfaces, substantially affecting water oxidation currents.[11,13,17–19] Thus, even for a well-understood water oxidation catalyst used as an electrocatalyst, understanding the catalyst-photoanode interaction is critical to enhance photocurrent yields in metal oxide/electrocatalyst photoanodes.

Several earth abundant and inexpensive electrocatalysts have garnered extensive attention for water oxidation, such as cobalt based CoPi,[20] and Co-Fe Prussian Blue.[14] Transition metal oxyhydroxides (referred to herein as MOOH) like NiOOH and FeOOH have also been coupled with $BiVO_4$ and some of these combinations have resulted in the construction of state-of-the-art $BiVO_4$ photoanodes,[13,15,21] exhibiting remarkable photocurrent densities of 5.87 mA/cm^2 at 1.23 V_{RHE}.[15] However, while the presence of MOOH considerably enhances the water oxidation performance of $BiVO_4$, most notably for nanoporous electrodes, the origin of this enhancement has not been clearly elucidated to date. Crucially, it has also been observed that the performance enhancement of the $BiVO_4$/MOOH system using either FeOOH or NiOOH for water oxidation does not correlate with the performance of FeOOH or NiOOH, respectively, when used as electrocatalysts on FTO.[13] This discrepancy complicates the optimisation of photoelectrochemical devices and highlights the need to improve our understanding of photoanode/electrocatalyst interface.[13]

In this study, transient optical and spectroelectrochemical techniques are utilised to: (1) compare performances of FeOOH, NiOOH, FeOOHNiOOH in terms of when they are used as an electrocatalyst on a conducting substrate in neutral electrolyte; and (2) investigate how their performance changes

they are placed on $BiVO_4$ nanoporous photoanodes and need to utilise photogenerated holes for water oxidation under the same electrolyte conditions. The results obtained from this study provide insight into the role of MOOH on $BiVO_4$ in enhancing water oxidation photocurrent and in the performance differences of the three MOOH catalysts on a conducting substrate and on a $BiVO_4$ photoelectrode.

Results and Discussion

Nanoporous $BiVO_4$ photoanodes used in this study were prepared using previously reported methods with one modification (see Supporting Information for details),[13] which was decreasing the film thickness (from ~750 to ~450-500 nm). This was necessary to increase the transparency of the $BiVO_4$ photoanodes, which is critical for the spectroscopic methods used in this study. As a result, the photocurrent obtained in this study with thinner $BiVO_4$ photoanodes is lower than that previously reported.[13] However, this decrease did not affect our comparison of the interactions of $BiVO_4$ with various MOOH electrocatalysts.

The FeOOH, NiOOH, FeOOHNiOOH electrocatalysts were synthesised as previously reported by anodic deposition on FTO to examine electrocatalytic function[22] and on $BiVO_4$ to examine photoelectrocatalytic function.[13] The trend in the photoelectrochemical enhancements between the three electrocatalysts upon when deposited on nanoporous $BiVO_4$ has previously been reported.[13] When deposited on FTO, the thicknesses of the FeOOH and NiOOH electrocatalysts were determined to be ~ 80 nm.[22] The FeOOHNiOOH, which was prepared by sequential deposition of FeOOH and NiOOH layers, was ~120 nm thick.[22] When deposited onto $BiVO_4$, the thickness of the catalyst layer was < 5 nm for FeOOH or NiOOH and < 10 nm for FeOOHNiOOH (increasing the thickness of the electrocatalyst layer on $BiVO_4$ is not favourable for photocurrent generation[13]). We note that NiOOH in this study was deposited, as previously, in an electrolyte that was not rigorously free of Fe impurities, and the NiOOH contained a trace amount of Fe (~1 at %).[22] Thus, hereafter, NiOOH will be denoted as Ni(Fe)OOH.

All investigations presented herein were performed at pH 7 as the current work aims to better understand the high performance of $BiVO_4$/MOOH photoanodes reported previously at this pH.[13] While MOOH electrocatalysts are typically used in basic conditions, MOOH-coupled photoanodes that are not stable in strongly basic conditions, such as $BiVO_4$, are often used in (near) neutral conditions to optimise system stability.

At pH 7, the three MOOH electrocatalysts studied herein exhibit similar electrochemical water oxidation performances, as can be seen in the steady-state current voltage (J – V) plots shown in *Figure*

1a. The similar overall performance at pH 7 differs from that observed under alkaline media (pH 13), where the catalytic onset potential for FeOOH is anodically shifted by 70 mV compared with Ni(Fe)OOH and FeOOHNiOOH.[22] All the presented studies for NiOOH and FeOOHNiOOH and their photoanode counterparts were obtained after the in situ regeneration of NiOOH from $Ni(OH)_2$, using an activation procedure detailed previously,[22] as $Ni(OH)_2$ forms over time when the electrodes are not in use (see Supporting Information for details). This activation process is referred to herein as the **(0/+)** oxidation process.

When these catalysts are deposited on top of $BiVO_4$ photoanodes remarkable enhancements in the photoelectrochemical water oxidation performance are observed in comparison to the unmodified nanoporous $BiVO_4$ photoanode (Figure 1b). To understand the origin of this performance enhancement upon MOOH addition, transient optical and spectroelectrochemical techniques were employed to compare the water oxidation and recombination kinetics of the Ni/Fe oxyhydroxide water oxidation electrocatalysts when used either as electrocatalyst or when deposited on $BiVO_4$ photoanodes.

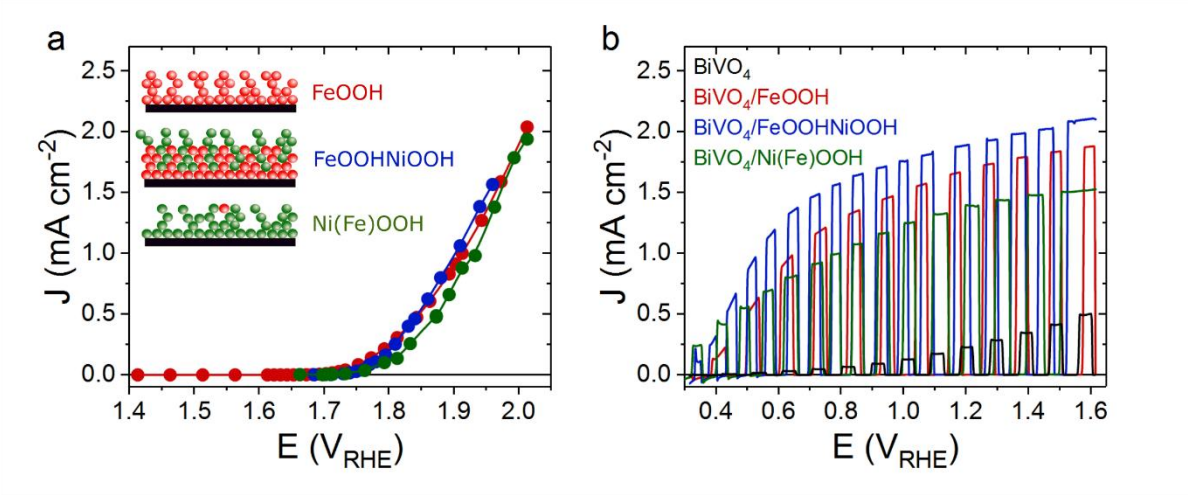

Figure 1. Electrochemical and photoelectrochemical performance of FeOOH, FeOOHNiOOH as electrocatalyst and when functionalised on $BiVO_4$ photoanodes at pH 7. (a) Steady state J-V curves for FeOOH (red), FeOOHNiOOH (blue) and Ni(Fe)OOH (green); These were recorded by measuring the steady state current at different applied potential under atmospheric conditions. Inset: schematic representation of the different electrocatalyst samples studied in this work. Red represents a Fe-based group, and green represents a Ni-based group. (b) Linear Sweep Voltammetry (LSV) under chopped light (1 sun equivalent, 365 nm LED, back irradiation) for $BiVO_4$/FeOOH (red), $BiVO_4$/FeOOHNiOOH (blue), $BiVO_4$/Ni(Fe)OOH (green) and un-modified $BiVO_4$ (black). All measurements were conducted in 0.1 M phosphate buffer. The J - V curves were recorded using a 10 mV/s scan rate.

Firstly, the optical and kinetic characteristics of the electrocatalysts when deposited on FTO were analysed. The optical changes during the sample activation **(0/+)** oxidation process to convert $Ni(OH)_2$

to NiOOH for both Ni(Fe)OOH and FeOOHNiOOH electrocatalyst samples are shown in *Figure* S2.[22–25] It is observed that Ni(Fe)OOH accumulated more **(0/+)** compared with FeOOHNiOOH. Since Ni(Fe)OOH and FeOOHNiOOH both contain similar amounts of NiOOH,[22] this result suggests that as the Fe content increases, the oxidation of $Ni(OH)_2$ to NiOOH becomes more difficult. This is consistent with previous literature where the shift in the oxidation of $Ni(OH)_2$/NiOOH to more anodic potentials has been correlated with the increase in Fe content.[24,26]

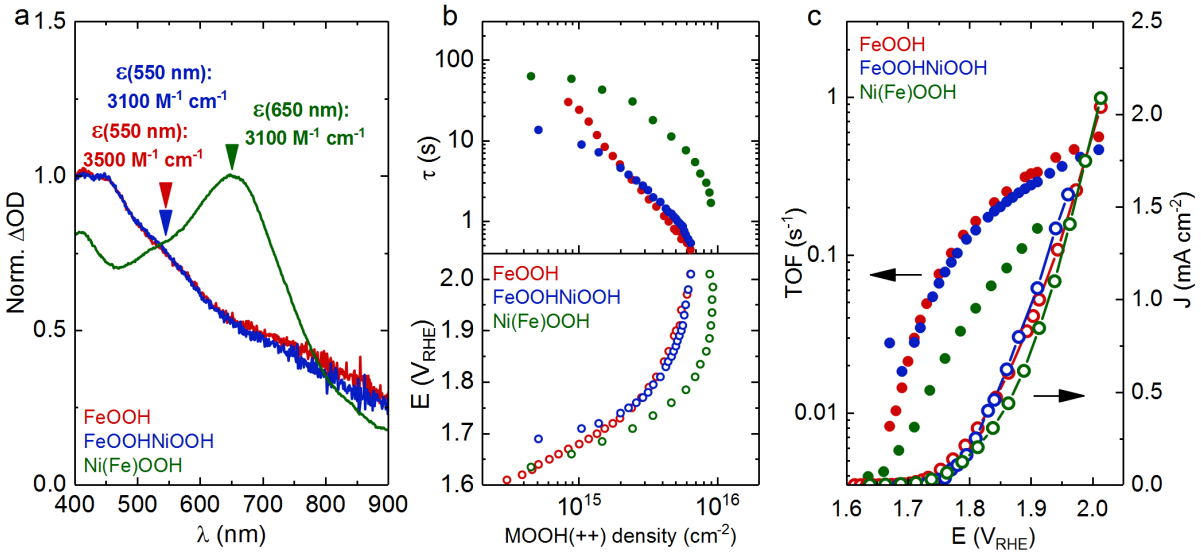

Figure 2. Kinetics of water oxidation under electrochemical conditions by the FeOOH, FeOOHNiOOH and Ni(Fe)OOH electrocatalysts. (a) Normalised ΔOD spectra of the MOOH(++) species and their corresponding extinction coefficient for FeOOH (red), FeOOHNiOOH (blue) and Ni(Fe)OOH (green). The spectra are obtained by subtracting the spectra after activation from the spectrum at 1.81 V_{RHE}. (b) Water oxidation reaction time constants (τ, solid circles, top panel) and the applied potential (bottom panel) as a function of the accumulated MOOH(++) density. (c) The TOF for O_2 evolution (solid circles, left axis) against the applied potential, plotted together with the current density (open circles, right axis). All measurements were taken in 0.1 M phosphate buffer (pH 7). Same colours used in (a), (b) and (c).

Figure 2a shows the optical response of the electrocatalysts. At applied potentials greater than the water oxidation catalytic onset, growth of new spectral features can be observed for each of the electrocatalysts, as shown in *Figure* 2a (and *Figure* S3 for spectra as a function of applied potential). These spectral features are assigned to the generation of oxidised states that accumulate under water oxidation catalysis, referred to as MOOH(++) herein. As can be observed in *Figure* 2a (blue and red traces), the spectra of the FeOOH(++) and the FeOOHNiOOH(++) species are almost indistinguishable, with an absorption maximum between 400 – 425 nm, suggestive of the similar nature of these oxidised states. In contrast, the Ni(Fe)OOH(++) species shown in *Figure* 2a (green trace) exhibit a peak centred

at ~650 nm, indicative of a different nature of the oxidised state that forms in Ni(Fe)OOH. A similar trend for the respective spectral features of the MOOH(+) and MOOH(++) species of these three electrocatalysts, is also present at pH 13,[22] suggesting that the catalytically active species observed under neutral and alkaline conditions are similar in nature. It is worth noting that the Ni(Fe)OOH samples were found to be relatively unstable when potentials greater than 2 V_{RHE} were applied, leading to a loss in the optical signal and performance. This effect can be associated with the gradual dissolution of NiOOH at pH 7 under anodic bias required for water oxidation (see Supporting Information for more details, *Figures S3 – S5*).[27]

To allow quantitative comparison of the oxidation of these electrocatalysts and the associated water oxidation kinetics, the extinction coefficients (ε) of the MOOH(++) oxidised species for each of the catalysts shown in *Figure 2a* were estimated using step-potential spectroelectrochemistry (SP-SEC), (see *section D* in Supporting Information for description of the method and additional data). Extinction coefficient (ε) values of ~3500 and ~3100 $M^{-1}\,cm^{-1}$ were obtained at wavelengths of 550 nm for FeOOH and FeOOHNiOOH, and a value of ~3100 $M^{-1}\,cm^{-1}$ was obtained at 650 nm for Ni(Fe)OOH. Using the estimated values of ε for each of the samples, the optical signal (ΔOD) shown in *Figure S3* can be correlated with the density of accumulated MOOH(++) species as a function of applied potential. When combined with current densities, these data yield kinetic information on the water oxidation process, allowing the estimation of reaction time (τ) or turn over frequency (TOF) for O_2 evolution, as a function of MOOH(++) species. These analyses have been described in *section F* in the Supporting Information and have been reported previously.[22] The water oxidation kinetic data are plotted as a function of MOOH(++) accumulated species (*Figure 2b*) and also as a function of applied potential (*Figure 2c*).

As can be observed in *Figure 2b* (empty circles, bottom panel), the density of the MOOH(++) accumulated species increases with the applied potential for each of the electrocatalysts, resulting in an acceleration of the water oxidation time constants (τ) by two orders of magnitude (solid circles, top panel). For a given potential, it is also observed that Ni(Fe)OOH accumulates more MOOH(++) species than FeOOH and FeOOHNiOOH. Whilst it is apparent that both FeOOH and FeOOHNiOOH exhibit similar reaction time constants, Ni(Fe)OOH(++) states oxidise water circa an order of magnitude more slowly, when compared at equivalent densities of MOOH(++) species. The slower water oxidation kinetics of Ni(Fe)OOH(++) is also reflected in the plot of TOF(s^{-1}) vs applied potential (*Figure* 2c) which shows that at a given potential, FeOOH(++) and FeOOHNiOOH(++) both oxidise water at a similar rate, whereas the TOF (s^{-1}) for Ni(Fe)OOH(++) is approximately halved. Overall, while Ni(Fe)OOH(++) is able to accumulate a greater density of MOOH(++) species than FeOOH and FeOOHNiOOH, this gain is offset by slower water oxidation kinetics. As a result, the electrocatalytic performance for water

oxidation is relatively invariant for all three electrocatalyst as shown in *Figure 1a* and *2c*. These trends are markedly different to those observed at pH 13 where Ni(Fe)OOH shows the fastest water oxidation kinetics amongst the three and, in comparison to FeOOHNiOOH, FeOOH starts accumulating charge at more anodic potentials, consistent with a later catalytic onset.[22] However the origin of these differences with pH is beyond the scope of this study.

Next we look at the interaction between these electrocatalyst and $BiVO_4$ photoanodes. The poor performance of the un-modified nanoporous $BiVO_4$ has previously been assigned to holes accumulating at the $BiVO_4$ surface undergoing extensive losses due to water oxidation kinetics on $BiVO_4$ being slower than surface recombination.[13] However it was not clear if the performance enhancement observed after addition of MOOH results primarily from faster water oxidation kinetics or slower surface recombination kinetics.

The enhancement observed in Figure 1b is consistent with that reported previously for these $BiVO_4$/MOOH combinations[13,15] and is much greater than that typically found when electrocatalysts (e.g. CoPi) are deposited on dense planar $BiVO_4$ electrodes;[11,28] such comparisons between CoPi and MOOH electrocatalysts are discussed later. Interestingly, while the three MOOH electrocatalysts show comparable performances, the $BiVO_4$/MOOH photoelectrodes exhibit differences in their water oxidation photocurrents (*Figure* 1b). In order to unravel the origin of the differences in performance enhancement upon the addition of MOOH electrocatalysts to $BiVO_4$, two different time-resolved optical and photoelectrochemical techniques are employed: transient absorption spectroscopy (TAS) employing short laser pulse excitation, and spectroelectrochemical photo-induced absorption spectroscopy (PIAS), employing quasi-steady state LED excitation.

To investigate if charge transfer occurs following bandgap excitation of $BiVO_4$, TAS was employed under an applied potential of 1.4 V_{RHE}. *Figure 3a* and *b* presents the TA spectra for $BiVO_4$ and $BiVO_4$/Ni(Fe)OOH and a comparison of the normalised charge carrier kinetics between un-modified $BiVO_4$ and the $BiVO_4$/Ni(Fe)OOH photoanodes. Equivalent TA spectra for the other $BiVO_4$/MOOH configurations are included in the Supporting Information (*Figure* S8). The data for $BiVO_4$ are similar to that reported previously, and are associated with holes accumulated at the surface.[29] The optical signal observed at shorter wavelengths (~<500 nm) across all $BiVO_4$ and $BiVO_4$/MOOH photoanodes is dominated by a short-lived transient bleach and is indicative of the trapping of conduction band electrons into oxygen vacancy states as reported previously (we note that the magnitude of this bleaching varies between samples, mostly likely resulting from differences in oxygen vacancy density).[30] The recovery of the bleach in the optical signal on the 1 ms timescale is concomitant with

the electron extraction from the photoanodes, after which only the longer lived optical signal for $BiVO_4$ holes or MOOH(++) species can be observed.[30]

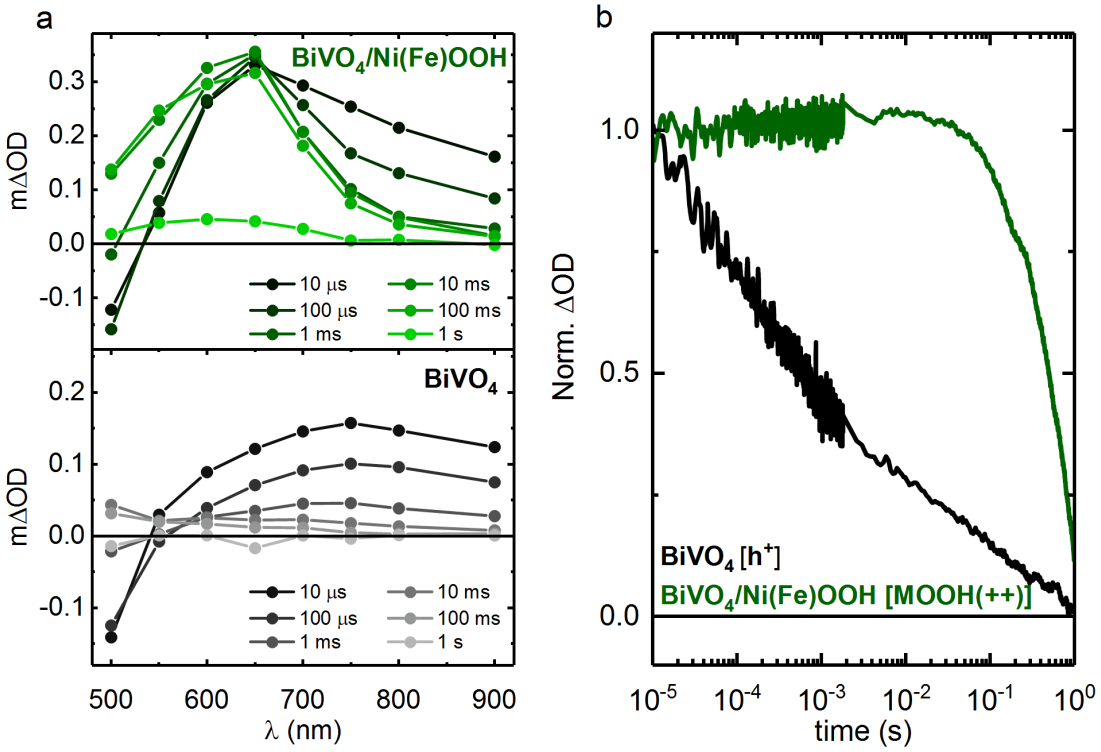

Figure 3. Transient absorption spectra and kinetics of $BiVO_4$ and $BiVO_4$/Ni(Fe)OOH photoanodes. (a) The transient absorption spectra showing the spectral signature of Ni(Fe)OOH(++) species in $BiVO_4$/Ni(Fe)OOH (top panel) and $BiVO_4$ (bottom panel). (b) Normalised transient absorption kinetics of $BiVO_4$ (black, 650 nm, h^+) and $BiVO_4$/Ni(Fe)OOH (green, 650 nm, Ni(Fe)OOH(++)). All data were obtained under an applied potential of 1.4 V_{RHE}, using 355 nm excitation (300 µJ/cm^2), in 0.1 M phosphate buffer.

In the case of $BiVO_4$/Ni(Fe)OOH (*Figure 3a*, top panel), a peak at 650 nm can be observed from the 10 µs TA spectra onwards, which is reminiscent of the Ni(Fe)OOH(++) species observed under electrocatalytic conditions shown in *Figure* 2a. This similarity in the spectral features at 650 nm suggest that both electrical and photo-induced oxidation (via surface holes from $BiVO_4$) generate similar Ni(Fe)OOH(++) species. The observation of this feature in the spectrum obtained at 10 µs is indicative of a significant fraction of fast hole transfer from $BiVO_4$ to the MOOH catalyst, which occurs within the time resolution of the measurements (< 10 µs). The spectral shape in *Figure* 3a (top panel) is clearly distinct from un-modified $BiVO_4$ (*Figure 3a*, bottom panel) at all timescales, indicating that holes primarily reside in the Ni(Fe)OOH catalyst layer over the timescales studied herein. Comparison of the kinetic traces presented in *Figure* 3b shows that Ni(Fe)OOH(++) species have a much longer lifetime than the holes in $BiVO_4$. Following hole transfer from $BiVO_4$ to the Ni(Fe)OOH layer, the accumulated Ni(Fe)OOH(++) species are spatially separated from photogenerated electrons in $BiVO_4$

and therefore, surface recombination in $BiVO_4$/Ni(Fe)OOH is reduced in comparison to un-modified $BiVO_4$. Analogous conclusions can be drawn for the cases of $BiVO_4$/FeOOH and $BiVO_4$/FeOOHNiOOH, where the spectral profiles of the MOOH(++) species can be observed in the TA spectra (millisecond onwards), although charge transfer is less clear than the case of $BiVO_4$/Ni(Fe)OOH due to the similarity in the spectral signatures of holes in $BiVO_4$ and MOOH(++) species in FeOOH and FeOOHNiOOH within the probed region. In addition, the optical signature of MOOH(++) species for FeOOH and FeOOHNiOOH at early timescales (µs – ms) also overlaps with the transient bleach observed due to electron trapping in $BiVO_4$, further obscuring the detection of charge transfer at early timescales for these two cases. Nonetheless, all three catalyst-functionalised samples exhibit much longer lived signals than $BiVO_4$ alone (as seen in the TA spectra, *Figure 3* and *Figure* S8 in the SI), indicative of catalyst deposition resulting in a substantial extension of the lifetime of photogenerated charges, attributed to slower recombination kinetics.

At early timescales (between 10 µs and 1 ms), an absorption tail at longer wavelengths (~700 – 900 nm) is present in all samples (*Figure 3a and Figure S8*). As this spectral signal is also present in the un-modified $BiVO_4$ photoanode, it may be indicative of photogenerated charges within $BiVO_4$. In the case of the catalyst modified samples ($BiVO_4$/MOOH), this tail absorption decays by ~1 ms without any significant concomitant change in the signal observed for the MOOH(++) species, most clearly visible for the case of $BiVO_4$/Ni(Fe)OOH (*Figure 3a)*. Since the extinction coefficients of the MOOH(++) species are ~7-8 times larger than the hole extinction coefficient of $BiVO_4$ (420 M^{-1} cm^{-1})[28], any further hole transfer from $BiVO_4$ to the catalyst layer within 10 µs and 1 ms would be expected to give rise to a much larger signal observed for the MOOH(++) species. Since no increase in signal is observed, this may be indicative of recombination of photogenerated species in $BiVO_4$ that have not transferred to the catalyst layer by ~10 µs.

It is intriguing that the FeOOHNiOOH functionalised $BiVO_4$ photoanode performs better than the FeOOH counterpart (*Figure* 1b), despite exhibiting almost invariant kinetics for water oxidation under electrocatalytic conditions (*Figure* 2b). From the TA spectra (*Figure* S8), it appears that the signal amplitude for $BiVO_4$/FeOOHNiOOH is slightly larger than it is for $BiVO_4$/FeOOH. Taking the respective extinction coefficients of the MOOH(++) species into consideration, this would indicate that a greater amount of holes successfully transfer from $BiVO_4$ to FeOOHNiOOH in comparison to FeOOH , thus suggestive of FeOOHNiOOH being able to accumulate a greater density of MOOH(++) in comparison to FeOOH alone, when deposited on $BiVO_4$. On the other hand, the lower performance of $BiVO_4$/Ni(Fe)OOH can be explained by the slower kinetics of the Ni(Fe)OOH(++) species (as shown in *Figure* 2b) for the same accumulated charges. For electrochemical water oxidation, this is

compensated by the accumulation of a greater density of MOOH(++) species. However, under illumination when $BiVO_4$/Ni(Fe)OOH is used, the maximum number of charges accumulated on the Ni(Fe)OOH layer will be determined primarily by the number of photogenerated holes that are transferred to the catalyst layer. As observed in the TA spectra at early timescales, the amount of MOOH(++) accumulated on the MOOH layer is within the same order of magnitude between the three catalysts. Since water oxidation is slower on Ni(Fe)OOH in comparison to the other two catalysts for a given MOOH(++) density, there is increased scope for competing recombination processes at the $BiVO_4$/Ni(Fe)OOH interface, as reported previously.[18]

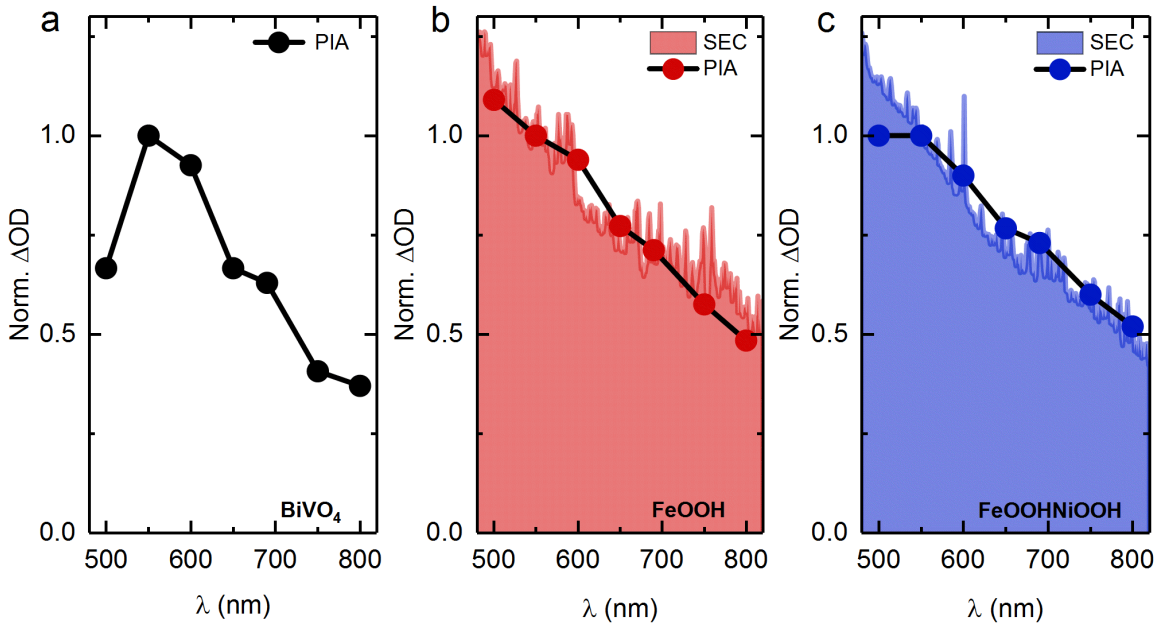

Figure 4. Comparison of normalised spectra of MOOH(++) species under electrochemical (EC) and photoelectrochemical (PEC) conditions. (a) The PIA spectrum of $BiVO_4$. (b) The SEC spectrum of FeOOH electrocatalyst (red, shaded) and the PIA spectrum of $BiVO_4$/FeOOH (solid red circle, black line). (c) The SEC spectrum of FeOOHNiOOH electrocatalyst (blue, shaded) and the PIA spectrum of $BiVO_4$/FeOOHNiOOH (solid blue circle, black line). All SEC spectra under electrochemical conditions were obtained under an applied potential of 2 V_{RHE}, and all PIA spectra were obtained under 1 sun equivalent illumination (365 nm LED) under 1.4 V_{RHE}. All spectra were normalised at 550 nm. All measurements were taken in 0.1 M phosphate buffer (pH 7).

To examine the photoelectrochemical processes under steady-state conditions, spectroelectrochemical photoinduced absorption spectroscopy (PIAS) was employed. Unfortunately, instability of $BiVO_4$/Ni(Fe)OOH samples (*Figure S6*) under oxidative conditions over prolonged periods of time required for PIAS measurements precludes them from these analyses. The normalised PIAS spectra of $BiVO_4$, $BiVO_4$/FeOOH and $BiVO_4$/FeOOHNiOOH under an applied potential of 1.4 V_{RHE} and 1 sun illumination are shown in *Figure 4*, along with the normalised spectra of the respective MOOH(++) species obtained under electrochemical conditions. The resemblance of the spectral shapes indicate

that similar species accumulate under the two catalytic conditions, which, in conjunction with the TAS data discussed above, further confirms that photoexcitation of $BiVO_4$ leads to the oxidation of the catalyst, also under PEC operation.

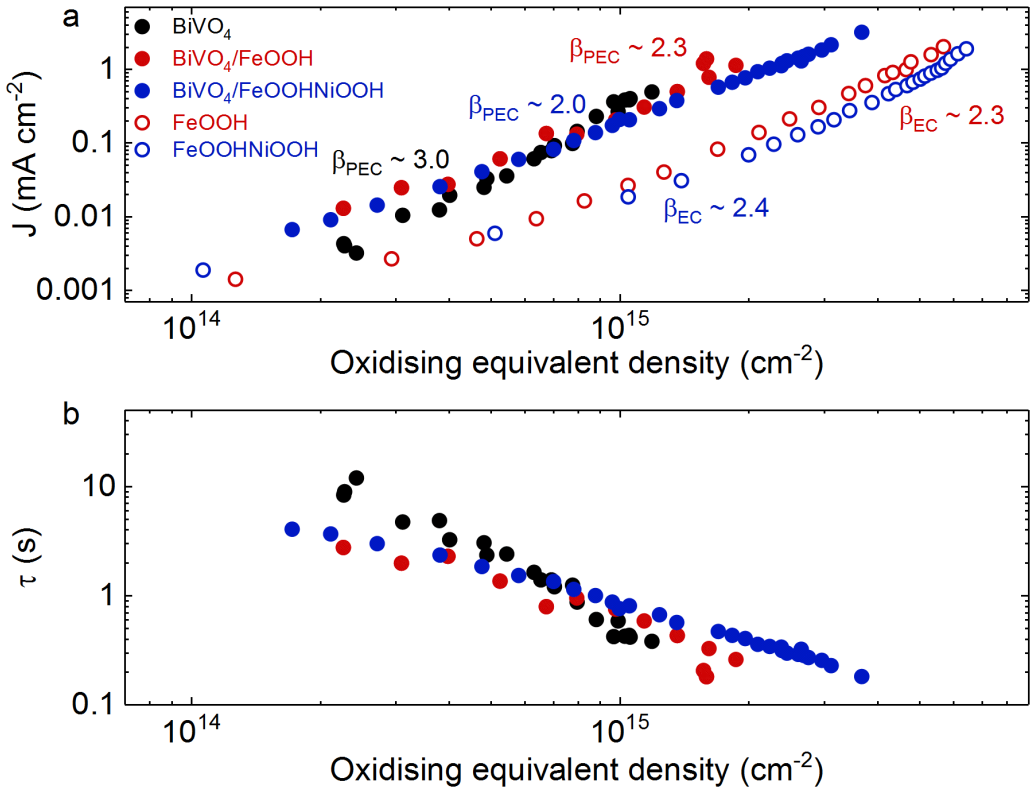

Figure 5. Comparison of kinetics under electrochemical and photoelectrochemical conditions. (a) The density of oxidising equivalents (h^+ for $BiVO_4$, or MOOH(++) species for catalysts) under catalytic conditions plotted against the (photo)current obtained. The reaction orders (β) for the respective electrochemical and photoelectrochemical water oxidation reactions are also shown (determined from the slope). (b) The density of oxidising equivalents plotted against the water reaction time constants (τ) under photoelectrochemical conditions for $BiVO_4$ and $BiVO_4$/MOOH photoanodes. Same colours used in (a) and (b): $BiVO_4$ (black solid circles); $BiVO_4$/FeOOH (red solid circles); $BiVO_4$/FeOOHNiOOH (blue solid circles); FeOOH (red empty circles); FeOOHNiOOH (blue empty circles). All measurements were taken in 0.1 M phosphate buffer.

The optical signals obtained through PIAS and SP-SEC for the photoanodes and electrocatalyst electrodes, respectively, under catalytic conditions, were converted to the amount of oxidising equivalents for water oxidation, *i.e.* holes in $BiVO_4$ and MOOH(++) species in the case of the catalysts. By relating the optical signal to the concomitant current transient signals, kinetic information associated with water oxidation reaction can be analysed using rate law plots according to the following equation:

$$\log J = log k_{WO} + \beta \log (\mathrm{MOOH}(++)) \qquad (1)$$

Where *J* is the (photo)electrochemical steady-state current density (water oxidation flux), (MOOH(++)) is the density of the MOOH(++) species (in the case of un-modified $BiVO_4$, it is the surface h^+ density), k_{WO} is the water oxidation rate constant and β is the order of the reaction with respect to the surface density of MOOH(++) (or h^+ density in $BiVO_4$). This analysis approach has been employed to investigate reaction kinetics on metal oxide surfaces[31–33] and electrocatalytic systems previously.[22,34]

Firstly, from *Figure* 5a, we can observe that photogenerated holes in $BiVO_4$ follow a reaction order (β) of 3 for water oxidation, consistent with previous reports,[31,32] whereas both FeOOH and FeOOHNiOOH operate with a β value of ~2 under both photoelectrochemical and electrochemical conditions at pH 7. A reaction order of ~2 for these electrocatalysts differs from that observed under alkaline conditions (β ~4 at pH 13),[22] and is indicative of differences in reaction mechanisms in neutral and alkaline media. More importantly, at pH 7, the different reaction orders between $BiVO_4$ and $BiVO_4$/MOOH photoanodes indicates that the water oxidation reaction proceeds via different mechanisms when driven directly by photogenerated holes in $BiVO_4$ and by MOOH(++) species in the catalyst layer, where the MOOH(++) species are generated following hole transfer from $BiVO_4$. Furthermore, it is apparent that similar orders of magnitude of MOOH(++) species are observed optically under both electrochemical (EC) and photoelectrochemical (PEC) conditions, consistent with the MOOH(++) species driving water oxidation in both systems, although differences in film morphology between the EC and PEC samples prevent quantitative comparison. A comparison of the reaction time constants for PEC water oxidation, shown in *Figure* 5b for $BiVO_4$ and $BiVO_4$/MOOH photoelectrodes, indicate that no significant enhancement in water oxidation timescale is gained upon electrocatalyst deposition.

It is also striking that catalysts often employed for water oxidation, where water oxidation is observed to take place via oxidised states in the catalyst (*i.e.* Co-Fe based Prussian Blue), display time constants on the order of seconds.[35] Even the popular Ni(Fe)OOH catalysts investigated under optimal alkaline conditions[22] operate with time constants that are comparable to water oxidation by metal oxides such as $BiVO_4$, and slower than that observed for WO_3.[32,36] Therefore it appears that the significant enhancement in photoelectrochemical performance of $BiVO_4$ photoanodes decorated with these electrocatalysts does not originate from faster kinetics of water oxidation relative to $BiVO_4$. Rather, the results obtained in this study suggest that the role of the catalyst layer is to decrease the kinetics of surface recombination and effectively decrease the recombination losses via fast hole transfer from $BiVO_4$ to the catalyst layer. This spatially separates charges, and retards surface recombination losses that compete with water oxidation.

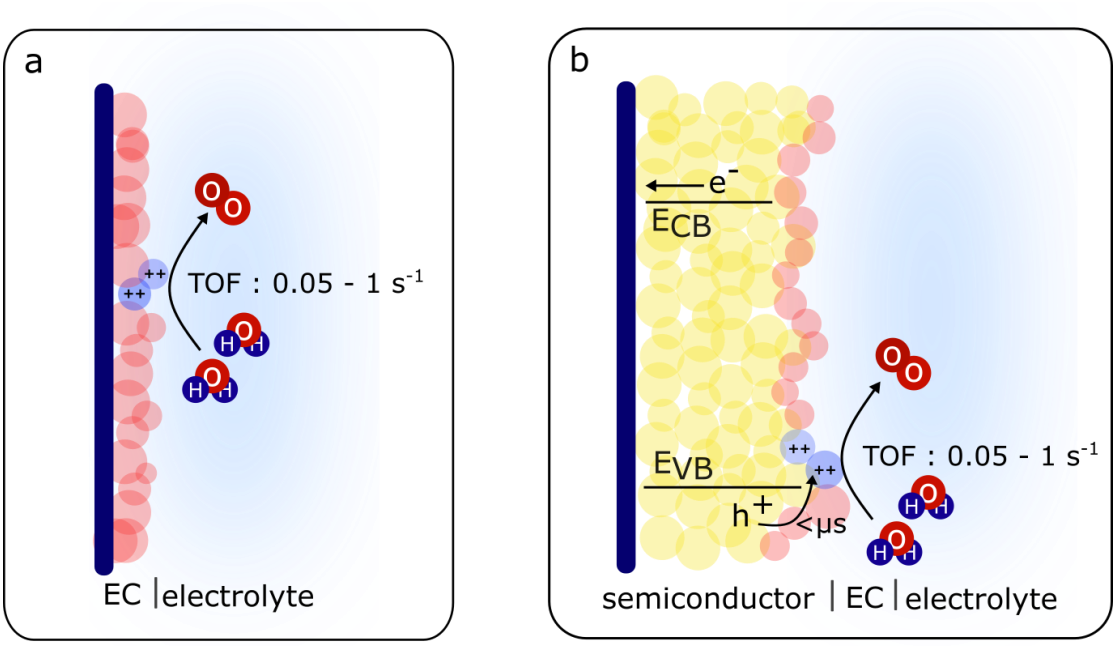

Scheme 1. Schematic illustration of electrochemical and photoelectrochemical water oxidation in MOOH electrodes and $BiVO_4$/MOOH photoelectrodes. (a) The electrochemically generated MOOH(++) species (blue spheres) in the activated electrocatalyst accumulate and drive water oxidation. (b) The photogenerated holes in the $BiVO_4$ transfer to the activated catalyst, generating MOOH(++) species (blue spheres) which then drive water oxidation. The electrons in the conduction band are collected at the back contact.

The same observations were found for Co-Fe Prussian Blue, where fast hole transfer to the catalyst layer followed by fast water oxidation kinetics led to enhanced performance.[35] This is however, markedly different to CoPi, which exhibits water oxidation time constants (τ) that are two to three orders of magnitude slower than what is observed for $BiVO_4$ alone, where the enhancement in performance has been attributed to increased band-bending within the $BiVO_4$ that drives charge separation.[17,28] It is observed that the amount of charge accumulated in CoPi under PEC conditions (when deposited on $BiVO_4$) is significantly lower (by two orders of magnitude) than that observed in the electrocatalyst under electrochemical water oxidation conditions at matched current densities.[28] Therefore, it is concluded that the amount of charge that accumulates in CoPi from $BiVO_4$ is insufficient to drive water oxidation. This conclusion is also supported by intensity-modulated photocurrent spectroscopy (IMPS) studies which indicate that CoPi mainly serves to passivate surface defects, with no significant enhancement of water oxidation kinetics when deposited on $BiVO_4$ or α-Fe_2O_3.[9,11] However, as conflicting studies based on dual working electrode measurements that assign water oxidation to the CoPi catalyst overlayers also have been reported,[37] this makes the role of CoPi as a co-catalyst overlayer on semiconductor photoelectrodes difficult to determine. For the case of the MOOH electrocatalysts studied herein, although a slight discrepancy in the amount of MOOH(++)

species is also observed between the electrocatalysts and the $BiVO_4$/MOOH photoelectrodes, this difference (within an order of magnitude) is less dramatic than the case of CoPi,[28] and is more similar to the case of RuO_x catalysts operating as electrocatalysts and co-catalysts on photoelectrochemical systems.[34] The charge transfer observed from $BiVO_4$ to the catalyst layer to generate MOOH(++) species is seen both in the transient absorption spectra and the photo-induced spectra under steady-state conditions. Additionally, as the reaction order for water oxidation for $BiVO_4$/MOOH photoanodes also differs from that of $BiVO_4$ photoanodes, it strongly indicates that water oxidation in the catalyst-decorated photoanodes studied herein is driven via MOOH(++) species accumulated in the catalyst layer (as illustrated in Scheme 1).

Conclusions

In this work, the electrochemical and photoelectrochemical performance of FeOOH, FeOOHNiOOH, and Ni(Fe)OOH catalysts are studied at pH 7 as standalone electrocatalysts and when added on the surface of $BiVO_4$ photoanodes. Our results demonstrate that electrocatalytic performance results from both the intrinsic reaction kinetics and the potential dependence of charge accumulation, where the latter consideration is not important under photoelectrochemical conditions. We show that while FeOOH and FeOOHNiOOH exhibit faster kinetics for water oxidation than Ni(Fe)OOH, this nickel-based catalyst is able to accumulate a larger density of oxidative MOOH(++). As a result, the three catalyst show a similar electrocatalytic water oxidation performances. This trade-off between accumulation and reaction kinetics hinders the selection of electrocatalysts to make junctions with photoanodes, through standard J-V characterisations.

Once deposited onto the surface of nanoporous $BiVO_4$ photoanodes, substantial improvements in the photoelectrochemical performance are observed with respect to un-modified $BiVO_4$, attributed to fast charge transfer (< 10 μs) from $BiVO_4$ to the catalyst layer, and the resultant suppressed recombination losses. However, rather surprisingly, no significant enhancement in the water oxidation time constant is observed for the $BiVO_4$/MOOH photoanodes in comparison to $BiVO_4$. Moreover, differences between the catalysts emerge in the $BiVO_4$/MOOH photoanodes, stemming from the charge accumulation within the catalyst layer being governed by the transfer of photogenerated holes from $BiVO_4$. This significantly impedes the ability of Ni(Fe)OOH to accumulate a greater amount of Ni(Fe)OOH(++) needed to offset its slower water oxidation kinetics, which leads to a lower performance of $BiVO_4$/Ni(Fe)OOH photoanodes in comparison to the other two configurations. On the other hand, when NiOOH is added to FeOOH as a dual-layer catalyst on $BiVO_4$, it helps accumulate more MOOH(++) species within the catalyst layer than FeOOH alone, resulting in a greater enhancement in the photocurrent generated by $BiVO_4$/FeOOHNiOOH photoanodes. Overall, this study

highlights the two different factors that govern the performance $BiVO_4$/MOOH photoanodes and need to be considered when selecting electrocatalysts for applications in photoelectrochemical systems: (1) the number of charges that can be accumulated within the catalyst layer; and (2) how fast these charges can oxidise water to compete with recombination processes.

Acknowledgements

J.R.D. and E.P. acknowledges financial support from the European Research Council (project Intersolar 291482). This project has received funding from the European Union's Horizon 2020 research and innovation program under grant agreement 732840-A-LEAF. C.A.M thanks COLCIENCIAS (now Ministry of Science, Technology and Innovation, call 568) for funding, L.F. thanks the EU for a Marie Curie fellowship (658270), S.S. thanks the EPRSC for a DTP scholarship and S.C. thanks Imperial College London for a Schrödinger Scholarship. K.-S.C. acknowledges financial support by the National Science Foundation under CHE-1764399.

References

(1) Barber, J.; Tran, P. D. From Natural to Artificial Photosynthesis. *J. R. Soc. Interface* **2013**, *10* (81). https://doi.org/10.1098/rsif.2012.0984.

(2) Andreiadis, E. S.; Chavarot-Kerlidou, M.; Fontecave, M.; Artero, V. Artificial Photosynthesis: From Molecular Catalysts for Light-Driven Water Splitting to Photoelectrochemical Cells. *Photochem. Photobiol.* **2011**, *87* (5), 946–964. https://doi.org/10.1111/j.1751-1097.2011.00966.x.

(3) Lewis, N. S.; Nocera, D. G. Powering the Planet: Chemical Challenges in Solar Energy Utilization. *Proc. Natl. Acad. Sci.* **2006**, *103* (43), 15729–15735. https://doi.org/10.1073/pnas.0603395103.

(4) Sivula, K.; van de Krol, R. Semiconducting Materials for Photoelectrochemical Energy Conversion. *Nat. Rev. Mater.* **2016**, *1* (2), 15010. https://doi.org/10.1038/natrevmats.2015.10.

(5) Yang, Y.; Niu, S.; Han, D.; Liu, T.; Wang, G.; Li, Y. Progress in Developing Metal Oxide Nanomaterials for Photoelectrochemical Water Splitting. *Adv. Energy Mater.* **2017**, *7* (19), 1–26. https://doi.org/10.1002/aenm.201700555.

(6) Xiao, M.; Luo, B.; Wang, Z.; Wang, S.; Wang, L. Recent Advances of Metal-Oxide Photoanodes: Engineering of Charge Separation and Transportation toward Efficient Solar Water Splitting. *Sol. RRL* **2020**, 1900509. https://doi.org/10.1002/solr.201900509.

(7) Cowan, A. J.; Tang, J.; Leng, W.; Durrant, J. R.; Klug, D. R. Water Splitting by Nanocrystalline TiO_2 in a Complete Photoelectrochemical Cell Exhibits Efficiencies Limited by Charge Recombination. *J. Phys. Chem. C* **2010**, *114* (9), 4208–4214. https://doi.org/10.1021/jp909993w.

(8) Le Formal, F.; Pendlebury, S. R.; Cornuz, M.; Tilley, S. D.; Grätzel, M.; Durrant, J. R. Back Electron–Hole Recombination in Hematite Photoanodes for Water Splitting. *J. Am. Chem. Soc.* **2014**, *136* (6), 2564–2574. https://doi.org/10.1021/ja412058x.

(9) Cummings, C. Y.; Marken, F.; Peter, L. M.; Tahir, A. A.; Wijayantha, K. G. U. Kinetics and

Mechanism of Light-Driven Oxygen Evolution at Thin Film α-Fe_2O_3 Electrodes. *Chem. Commun.* **2012**, *48* (14), 2027–2029. https://doi.org/10.1039/c2cc16382a.

(10) Peter, L. M.; Wijayantha, K. G. U.; Tahir, A. A. Kinetics of Light-Driven Oxygen Evolution at α-Fe_2O_3 Electrodes. *Faraday Discuss.* **2012**, *155* (0), 309–322. https://doi.org/10.1039/c1fd00079a.

(11) Zachäus, C.; Abdi, F. F.; Peter, L. M.; van de Krol, R. Photocurrent of $BiVO_4$ Is Limited by Surface Recombination, Not Surface Catalysis. *Chem. Sci.* **2017**, *8* (5), 3712–3719. https://doi.org/10.1039/C7SC00363C.

(12) Klahr, B.; Gimenez, S.; Fabregat-Santiago, F.; Bisquert, J.; Hamann, T. W. Photoelectrochemical and Impedance Spectroscopic Investigation of Water Oxidation with "Co-Pi"-Coated Hematite Electrodes. *J. Am. Chem. Soc.* **2012**, *134* (40), 16693–16700. https://doi.org/10.1021/ja306427f.

(13) Kim, T. W.; Choi, K.-S. Nanoporous $BiVO_4$ Photoanodes with Dual-Layer Oxygen Evolution Catalysts for Solar Water Splitting. *Science* **2014**, *343* (6174), 990–994. https://doi.org/10.1126/science.1246913.

(14) Hegner, F. S.; Herraiz-Cardona, I.; Cardenas-Morcoso, D.; López, N.; Galán-Mascarós, J. R.; Gimenez, S. Cobalt Hexacyanoferrate on $BiVO_4$ Photoanodes for Robust Water Splitting. *ACS Appl. Mater. Interfaces* **2017**, *9* (43), 37671–37681. https://doi.org/10.1021/acsami.7b09449.

(15) Wang, S.; Chen, P.; Bai, Y.; Yun, J.-H.; Liu, G.; Wang, L. New $BiVO_4$ Dual Photoanodes with Enriched Oxygen Vacancies for Efficient Solar-Driven Water Splitting. *Adv. Mater.* **2018**, *30* (20), 1800486. https://doi.org/10.1002/adma.201800486.

(16) Wang, D.; Li, R.; Zhu, J.; Shi, J.; Han, J.; Zong, X.; Li, C. Photocatalytic Water Oxidation on $BiVO_4$ with the Electrocatalyst as an Oxidation Cocatalyst: Essential Relations between Electrocatalyst and Photocatalyst. *J. Phys. Chem. C* **2012**, *116* (8), 5082–5089. https://doi.org/10.1021/jp210584b.

(17) Ma, Y.; Le Formal, F.; Kafizas, A.; Pendlebury, S. R.; Durrant, J. R. Efficient Suppression of Back Electron/Hole Recombination in Cobalt Phosphate Surface-Modified Undoped Bismuth Vanadate Photoanodes. *J. Mater. Chem. A* **2015**, *3* (41), 20649–20657. https://doi.org/10.1039/C5TA05826K.

(18) Hajibabaei, H.; Schon, A. R.; Hamann, T. W. Interface Control of Photoelectrochemical Water Oxidation Performance with $Ni_{1-x}Fe_xO_y$ Modified Hematite Photoanodes. *Chem. Mater.* **2017**, *29* (16), 6674–6683. https://doi.org/10.1021/acs.chemmater.7b01149.

(19) Zhong, D. K.; Choi, S.; Gamelin, D. R. Near-Complete Suppression of Surface Recombination in Solar Photoelectrolysis by "Co-Pi" Catalyst-Modified W:$BiVO_4$. *J. Am. Chem. Soc.* **2011**, *133* (45), 18370–18377. https://doi.org/10.1021/ja207348x.

(20) Kanan, M. W.; Nocera, D. G. In Situ Formation of an Oxygen-Evolving Catalyst in Neutral Water Containing Phosphate and Co^{2+}. *Science* **2008**, *321* (5892), 1072–1075. https://doi.org/10.1126/science.1162018.

(21) Lee, D. K.; Lee, D.; Lumley, M. A.; Choi, K. S. Progress on Ternary Oxide-Based Photoanodes for Use in Photoelectrochemical Cells for Solar Water Splitting. *Chem. Soc. Rev.* **2019**, *48* (7), 2126–2157. https://doi.org/10.1039/c8cs00761f.

(22) Francàs, L.; Corby, S.; Selim, S.; Lee, D.; Mesa, C. A.; Godin, R.; Pastor, E.; Stephens, I. E. L.; Choi, K.-S.; Durrant, J. R. Spectroelectrochemical Study of Water Oxidation on Nickel and Iron Oxyhydroxide Electrocatalysts. *Nat. Commun.* **2019**, *10* (1), 5208.

https://doi.org/10.1038/s41467-019-13061-0.

(23) Louie, M. W.; Bell, A. T. An Investigation of Thin-Film Ni-Fe Oxide Catalysts for the Electrochemical Evolution of Oxygen. *J. Am. Chem. Soc.* **2013**, *135* (33), 12329–12337. https://doi.org/10.1021/ja405351s.

(24) Gorlin, M.; De Araujo, J. F.; Schmies, H.; Bernsmeier, D.; Dresp, S.; Gliech, M.; Jusys, Z.; Chernev, P.; Kraehnert, R.; Dau, H.; et al. Tracking Catalyst Redox States and Reaction Dynamics in Ni-Fe Oxyhydroxide Oxygen Evolution Reaction Electrocatalysts: The Role of Catalyst Support and Electrolyte PH. *J. Am. Chem. Soc.* **2017**, *139* (5), 2070–2082. https://doi.org/10.1021/jacs.6b12250.

(25) Goldsmith, Z. K.; Harshan, A. K.; Gerken, J. B.; Vörös, M.; Galli, G.; Stahl, S. S.; Hammes-Schiffer, S. Characterization of NiFe Oxyhydroxide Electrocatalysts by Integrated Electronic Structure Calculations and Spectroelectrochemistry. *Proc. Natl. Acad. Sci. U. S. A.* **2017**, *114* (12), 3050–3055. https://doi.org/10.1073/pnas.1702081114.

(26) Trotochaud, L.; Young, S. L.; Ranney, J. K.; Boettcher, S. W. Nickel − Iron Oxyhydroxide Oxygen-Evolution Electrocatalysts : The Role of Intentional and Incidental Iron Incorporation. *J. Am. Chem. Soc.* **2014**, *136* (18), 6744–6753. https://doi.org/10.1021/ja502379c.

(27) Görlin, M.; Gliech, M.; De Araújo, J. F.; Dresp, S.; Bergmann, A.; Strasser, P. Dynamical Changes of a Ni-Fe Oxide Water Splitting Catalyst Investigated at Different PH. *Catal. Today* **2016**, *262*, 65–73. https://doi.org/10.1016/j.cattod.2015.10.018.

(28) Ma, Y.; Kafizas, A.; Pendlebury, S. R.; Le Formal, F.; Durrant, J. R. Photoinduced Absorption Spectroscopy of CoPi on $BiVO_4$: The Function of CoPi during Water Oxidation. *Adv. Funct. Mater.* **2016**, *26* (27), 4951–4960. https://doi.org/10.1002/adfm.201600711.

(29) Ma, Y.; Pendlebury, S. R.; Reynal, A.; Le Formal, F.; Durrant, J. R. Dynamics of Photogenerated Holes in Undoped $BiVO_4$ Photoanodes for Solar Water Oxidation. *Chem. Sci.* **2014**, *5* (8), 2964–2973. https://doi.org/10.1039/C4SC00469H.

(30) Selim, S.; Pastor, E.; García-Tecedor, M.; Morris, M. R.; Francàs, L.; Sachs, M.; Moss, B.; Corby, S.; Mesa, C. A.; Gimenez, S.; et al. Impact of Oxygen Vacancy Occupancy on Charge Carrier Dynamics in $BiVO_4$ Photoanodes. *J. Am. Chem. Soc.* **2019**, *141* (47), 18791–18798. https://doi.org/10.1021/jacs.9b09056.

(31) Ma, Y.; Mesa, C. A.; Pastor, E.; Kafizas, A.; Francàs, L.; Le Formal, F.; Pendlebury, S. R.; Durrant, J. R. Rate Law Analysis of Water Oxidation and Hole Scavenging on a $BiVO_4$ Photoanode. *ACS Energy Lett.* **2016**, *1* (3), 618–623. https://doi.org/10.1021/acsenergylett.6b00263.

(32) Mesa, C. A.; Francàs, L.; Yang, K. R.; Garrido-Barros, P.; Pastor, E.; Ma, Y.; Kafizas, A.; Rosser, T. E.; Mayer, M. T.; Reisner, E.; et al. Multihole Water Oxidation Catalysis on Haematite Photoanodes Revealed by Operando Spectroelectrochemistry and DFT. *Nat. Chem.* **2020**, *12* (1), 82–89. https://doi.org/10.1038/s41557-019-0347-1.

(33) Le Formal, F.; Pastor, E.; Tilley, S. D.; Mesa, C. A.; Pendlebury, S. R.; Grätzel, M.; Durrant, J. R. Rate Law Analysis of Water Oxidation on a Hematite Surface. *J. Am. Chem. Soc.* **2015**, *137* (20), 6629–6637. https://doi.org/10.1021/jacs.5b02576.

(34) Pastor, E.; Le Formal, F.; Mayer, M. T.; Tilley, S. D.; Francàs, L.; Mesa, C. A.; Grätzel, M.; Durrant, J. R. Spectroelectrochemical Analysis of the Mechanism of (Photo)Electrochemical Hydrogen Evolution at a Catalytic Interface. *Nat. Commun.* **2017**, *8*, 14280. https://doi.org/10.1038/ncomms14280.

(35) Moss, B.; Hegner, F. S.; Corby, S.; Selim, S.; Francàs, L.; López, N.; Giménez, S.; Galán-Mascarós,

J.-R.; Durrant, J. R. Unraveling Charge Transfer in CoFe Prussian Blue Modified $BiVO_4$ Photoanodes. *ACS Energy Lett.* **2018**, 337–342. https://doi.org/10.1021/acsenergylett.8b02225.

(36) Corby, S.; Francàs, L.; Selim, S.; Sachs, M.; Blackman, C.; Kafizas, A.; Durrant, J. R. Water Oxidation and Electron Extraction Kinetics in Nanostructured Tungsten Trioxide Photoanodes. *J. Am. Chem. Soc.* **2018**, *140* (47), 16168–16177. https://doi.org/10.1021/jacs.8b08852.

(37) Laskowski, F. A. L.; Nellist, M. R.; Qiu, J.; Boettcher, S. W. Metal Oxide/(Oxy)Hydroxide Overlayers as Hole Collectors and Oxygen-Evolution Catalysts on Water-Splitting Photoanodes. *J. Am. Chem. Soc.* **2019**, *141* (4), 1394–1405. https://doi.org/10.1021/jacs.8b09449.